academicJournals

Vol. 8(22), pp. 1209-1217, 16 June, 2013
DOI: 10.5897/IJPS12.576
ISSN 1992-1950 © 2013 Academic Journals
http://www.academicjournals.org/IJPS

International Journal of Physical Sciences

Full Length Research Paper

Polyaniline/Fe_3O_4 coated on $MnFe_2O_4$ nanocomposite: Preparation, characterization, and applications in microwave absorption

Seyed Hossein Hosseini[1]* and A. Asadnia[2]

[1]Department of Chemistry, Faculty of Science, Islamshahr Branch, Islamic Azad University, Tehran-Iran.
[2]Young Researchers Club, Center Tehran Branch, Islamic Azad University, Tehran-Iran.

Accepted 3 June, 2013

Conductive polyaniline (PANi)/Fe_3O_4 is coated on the $MnFe_2O_4$ nanocomposite with multi core shell structure was synthesized by in-situ polymerization in the presence of dodecyl benzene sulfonic acid (DBSA) as the surfactant and dopant and ammonium persulfate (APS) as the oxidant. The structure and magnetic properties of Fe_3O_4 coated on the $MnFe_2O_4$ nanoparticles were studied by using powder X-ray diffraction (XRD) and vibrating sample magnetometer (VSM), respectively. The morphology, microstructure and DC conductivity of the nanocomposite were characterized by scanning electron Microscopy (SEM), fourier transform infrared spectroscopy (FTIR) and four-wire-technique, respectively. The microwave absorbing properties of the nanocomposite dispersed in resin acrylic with thickness of 1.4 mm were investigated by a HP 8720B vector network analyzer and standard horn antennas in Anechoic chamber in the frequency range of 8–12GHz. A minimum reflection loss of -18 dB was observed at 8.6 GHz.

Key words: Nano-structures, polymer-matrix composites (PMCs), magnetic properties, microwave absorption (nominated).

INTRODUCTION

Microwave absorbing material plays a great role in electromagnetic pollution, electromagnetic interference (EMI) shielding and stealth technology, to name but a few. An‘‘ideal’’microwave absorbing material owns such advantages as low thickness, low density, wide band width and flexibility simultaneously (Hosseini et al., 2011). In the past decades, the spinel ferrites have been utilized as the most frequent absorbing materials in various forms. Manganeseferrite ($MnFe_2O_4$) is a common spinel ferrite material and has been widely used in microwave and magnetic recording applications (Xiao et al., 2006). The absorbing characteristics of the materials depend on the frequency, layer thickness, complex permittivity (ε_r) and complex permeability (μ_r). Fe_3O_4 is a kind of microwave absorbers with complex permittivity and complex permeability (Li et al., 2008a). The core-shell structure composite nanoparticles often exhibit improved physical and chemical properties over their single-component counterpart and hence are very useful in a broader range of applications (Zhang and Li, 2009). Conducting polymer composites with micro/nanostructures have attracted significant academic and technological attention because of their unique physical properties and potential applications in

*Corresponding author. E-mail: shhosseini@iiau.ac.ir.

nanoelectronics, electromagnetics, and biomedical devices. Among these conducting polymers composites decorated with organic nanoparticles are of particular interest because possible interactions between the inorganic nanoparticles and the polymer matrices may generate some unique physical properties upon the formation of various micro/nanocomposites (Yang et al., 2009). Among conducting polymers, polyaniline (PANi) is perhaps the most versatile because of easier and inexpensive preparation methods. Also they have desirable properties, such as thermal and chemical stability, low specific mass, controllable conductivity and high conductivity at microwave frequencies (Phang et al., 2008). PANi is a conducting polymer so it has many potential applications in various fields such as electrical – magnetic shields, microwave absorbing materials, batteries, sensors and corrosion protections. The development of PANi properties has received considerable attention lately. The fabrication of PANi /ferrite nanocomposite has been reported by using different methods such as in situ polymerization of aniline in the presence of $Zn_{0.6}Cu_{0.4}Cr_{0.5}Fe_{1.5}O_4$ nanoparticles, micro emulsion process used to prepare PANi/NiZn ferrite nanocomposite and oxidative electro – polymerization of aniline in an aqueous solution in the presence of MnZn ferrite and NiMnZn ferrite. These studies created organic materials possessing both conducting and ferromagnetic functions. The electromagnetic measurements of the PANi/ferrites were improved and tailored by controlling the addition of the ferrite in the composite. Also, the contribution of ferrite to the PANi led to an increase in its thermal stability, however, it was decreased it electrical conductivity (Farghali et al., 2010). The preceding work, we have investigated microwave absorbing property of PANi–manganese ferrite nanocomposite in the frequency range of 8–12 GHz. We showed the PANi–manganese ferrite nanocomposites are good electromagnetic wave absorbent in the microwave range (Hosseini et al., 2011).

EXPERIMENTAL

Materials and instrumentals

Chemicals including metal salts, hexamethylene tetraamine (HMTA), potassium persulfate (KPS), ammonium persulfate (APS) and ethylene glycol (EG), $FeCl_3 .6H_2 O$, $FeSO_4.H_2 O$, $NH_3.H_2O$ (28%), Oleic acid (90%), are analytical grade (Merck) and were used without further purification. Water was deionized, doubly distilled, and deoxygenated prior to use. Styrene and methacrylic acid (analytical grade, Merck) were distilled to remove the inhibitor. Aniline monomer (analytical grade, Merck) was distilled twice under reduced pressure. DBSA and acrylic resin were of industrial grade.

The morphology of coated particles and nanocomposite was observed scanning electron microscopy (SEM) with a JSM-6301F (Japan) instrument operated at an accelerating voltage of 10 kV. X-ray powder diffraction (XRD) patterns of the nanoparticles assembles were collected on a Philips-PW 1800 with Cu-K radiation under Cu Kα radiation (λ=1.5406 Å). Fourier transform infrared spectroscopy (FTIR) spectra were recorded on a PerkinElmer spectrum FTIR using KBr pellets. The M–H hysteresis loops were measured by vibrating sample magnetometer (VSM) (RIKEN DENSHI Co. Ltd., Japan). Microwave absorbing properties were measured by a HP 8720B vector network analyzer and standard horn antennas in anechoic chamber.

Synthesis of manganese ferrite ($MnFe_2O_4$) nanoparticles

In a typical experiment, 10 ml styrene, 2 ml methacrylic acid and 0.054 g KPS were added to the flask with 100 ml deionized water. To eliminate oxygen effects the solution was purged with nitrogen before the process was initiated. The mixture was heated to 72°C and stirred with a magnetic stirrer. The polymerization was continued for 24 h and in the whole procedure the nitrogen was purged. Concentration of PS spheres in solution is 80 mg/ml, which was calculated by drying 5 ml colloid solution and weighing the remained solids (Hosseini et al., 2011).

Synthesis of coated particles

The coating procedure consisted of controlled hydrolysis of ferrous chloride aqueous solutions and other divalent metal salts in the presence of polystyrene latexes. In a typical preparation process, 2 ml PS colloid solution was diluted with 250 ml deoxygenated distilled water and then mixed with the metal salts solution, which contained 10 mmol $FeCl_2$ and 5 mmol $MnCl_2$. After it dispersed under ultrasonic for several minutes, the mixture was in corporate with 4 g HMTA and 0.5 g potassium nitrate and heated to 85°C under gentle stirring. After 3 h, the system was cooled to room temperature. The solution was poured in to excess distilled water, then magnetic particles were deposited using magnetic field. The precipitate was washed with distilled water for several times and then dried in oven at 80°C for 24 h. In addition, to modify the surface chemical properties of the magnetic spheres, 5 ml ethylene glycol (EG) was added in to the reaction solution before the incorporation of HMTA.

Iron Ferrite (Fe_3O_4)

$FeCl_3.6H_2O$ (24.3 g) and $FeSO_4.7H_2O$ (16.7 g) were dissolved in 100 ml de-ionized water under nitrogen gas while stirring vigorously at 80°C. Then 50 ml of ammonium hydroxide were added rapidly into the solution. The color of the solution turned to black instantly. Oleic acid (3.76 g) was added 30 min later. Then the suspension was kept at 80°C for 1.5 h. The magnetite nanoparticles were washed with de-ionized water until the pH value of the system reached neutral. The as-synthesized sample was dried in vacuum at room temperature.

Preparation of Fe_3O_4 -coated on the $MnFe_2O_4$ ($MnFe_2O_4/Fe_3O_4$)

0.1 g nano-sized particles of prepared $MnFe_2O_4$ were dispersed in 200 ml water solution of pH 6 under ultra sonification for 2 min. At this pH, the surface charge of $MnFe_2O_4$ in the solution is expected to be positive, and that of Fe_3O_4 be negative. The two solutions were mixed at 1/19 volumetric ratio (1/19 weight ratio of $MnFe_2O_4$/ Fe_3O_4) and subjected to sonification for 2 min so that $MnFe_2O_4$ particles were coated with Fe_3O_4 particles. The solution was then filtered using ultrafiltration membrane and dried at room temperature. We also prepared physically mixed Fe_3O_4 and $MnFe_2O_4$ by mixing the two solid Fe_3O_4 and $MnFe_2O_4$ samples with 1/19 weight ratio of $MnFe_2O_4$/ Fe_3O_4 for 1 h using a rotating machine.

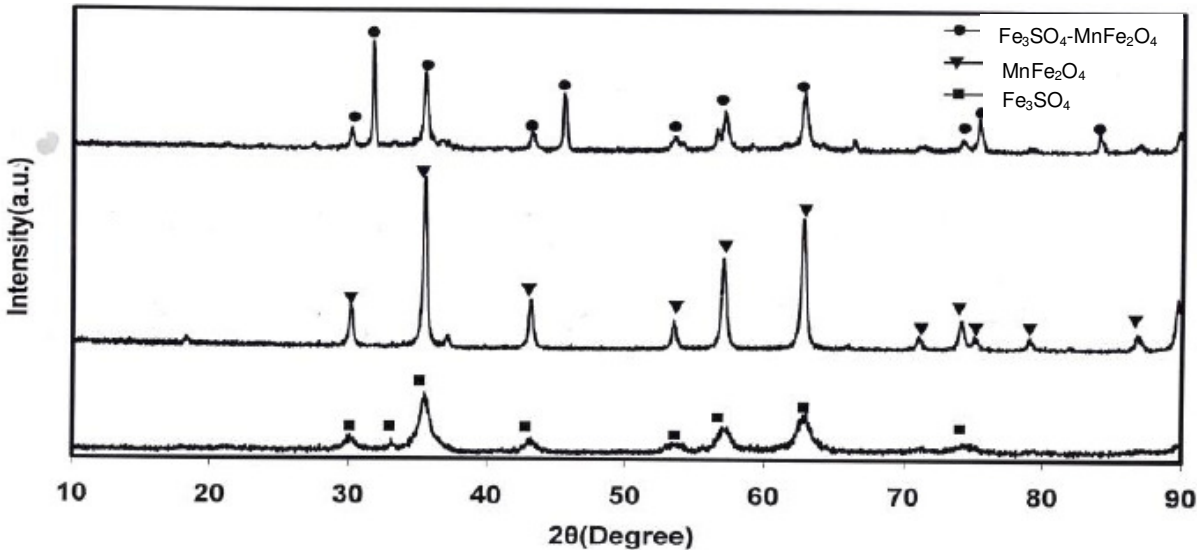

Figure 1. X-ray diffraction for Fe_3O_4, $MnFe_2O_4$ and $MnFe_2O_4/Fe_3O_4$ nanoparticles.

Synthesis of $MnFe_2O_4/Fe_3O_4$/PANi nanocomposite with multi core–shell structure

$MnFe_2O_4/Fe_3O_4$/PANi multi core–shell nanocomposites were prepared by in situ polymerization in the presence of DBSA as the surfactant and dopant and APS as the oxidant. The DBSA was dissolved in distilled water with vigorous stirring for about 20 min. The $MnFe_2O_4/Fe_3O_4$ nanoparticles (1.22 g) were added to the DBSA solution under stirring condition for approximately 1 h. Then 8 ml of aniline monomer was added to the suspension and stirred for 30 min. $MnFe_2O_4/Fe_3O_4$ nanoparticles were dispersed well in the mixture of aniline/DBSA under ultra sonicaction for 2 h. 20 g APS in 60 ml deionized water was gradually added drop wise to the stirred reaction mixture. Polymerization was allowed to proceed while stirring in an ice-water bath for 6 h. The nanocomposite was obtained by filtering and washing the suspension with deionized water and ethanol, respectively. The obtained green-black powder containing 15% $MnFe_2O_4/Fe_3O_4$ was dried under vacuum for 24 h.

RESULTS AND DISCUSSION

X-ray diffraction analysis

Figure 1 shows the XRD pattern of Fe_3O_4, $MnFe_2O_4$ and $MnFe_2O_4/Fe_3O_4$. According to the Figure, cubic ferrite Fe_3O_4 and $MnFe_2O_4$ nanoparticles have been obtained. However, it should be noted that there are some peaks of α-Fe_2O_3 in the XRD pattern for Fe_3O_4 (2θ=33,54) and $MnFe_2O_4$ (2θ=54) nanoparticles. All peaks correspond to the characteristic peaks of cubic type lattice for $MnFe_2O_4$ (JCPDS file no. 88-1965) and Fe_3O_4 (JCPDS file no. 19-0629). The obtained peak width from XRD patterns addresses to the sizes of nanoparticles. By using Debye–Scherrer equation, the sizes of $MnFe_2O_4$, Fe_3O_4 and $MnFe_2O_4/Fe_3O_4$ nanoparticles are calculated as 24.27, 7.38 and 31.65 nm, respectively. The XRD pattern indicates that $MnFe_2O_4/Fe_3O_4$ nanocomposites have formed. And compared with $MnFe_2O_4$ and Fe_3O_4 nanoparticles, the intensity of the characteristic peaks of α-Fe_2O_3 decreased in the $MnFe_2O_4/Fe_3O_4$ nanocomposites. This may be attributed to the coating of Fe_3O_4 nanoparticles on the surface of $MnFe_2O_4$ nanoparticles.

Magnetic properties

Magnetic properties of the samples were measured at room temperature with a VSM. The hysteresis loops are illustrated in Figure 2a-d. This Figure shows the magnetization (M) versus the applied magnetic field (H) for Fe_3O_4, $MnFe_2O_4$, $MnFe_2O_4/Fe_3O_4$ nanoparticles and d) $MnFe_2O_4/Fe_3O_4$/PANi nanocomposite (15 wt%) respectively. It can be inferred from the hysteresis loops that all the composite magnetic spheres are magnetically soft at room temperature with an applied field -10 kOe≤H≤10 kOe. Figure 2a shows the hysteresis loop of Fe_3O_4 (Hosseini et al., 2011). The value of saturation magnetization (M_s) is about 66.7 emu/g, the remnant magnetization (M_r) and the coercivity field are 17.81 emu/g and 110 Oe respectively. Figure 2b shows clear saturation magnetization (M_s) about 60 emu/g and remnant magnetization (M_r) and the coercivity field for $MnFe_2O_4$ nanocomposite are about 18 emu/g and 140 Oe respectively. The *Ms*, *Mr* and *Hc* are 37 emu/g, 11 emu/g and 155 Oe for $MnFe_2O_4/Fe_3O_4$ nanocomposite that have been shown in Figure 2c, respectively. It is lower than the pure ferrite manganese ferrite (Xiao et al., 2006) nanoparticles.

Although the $MnFe_2O_4/Fe_3O_4$ nanocomposites consist of two magnetic phases, the hysteresis loop shows a single-phase-like behavior, and the magnetization

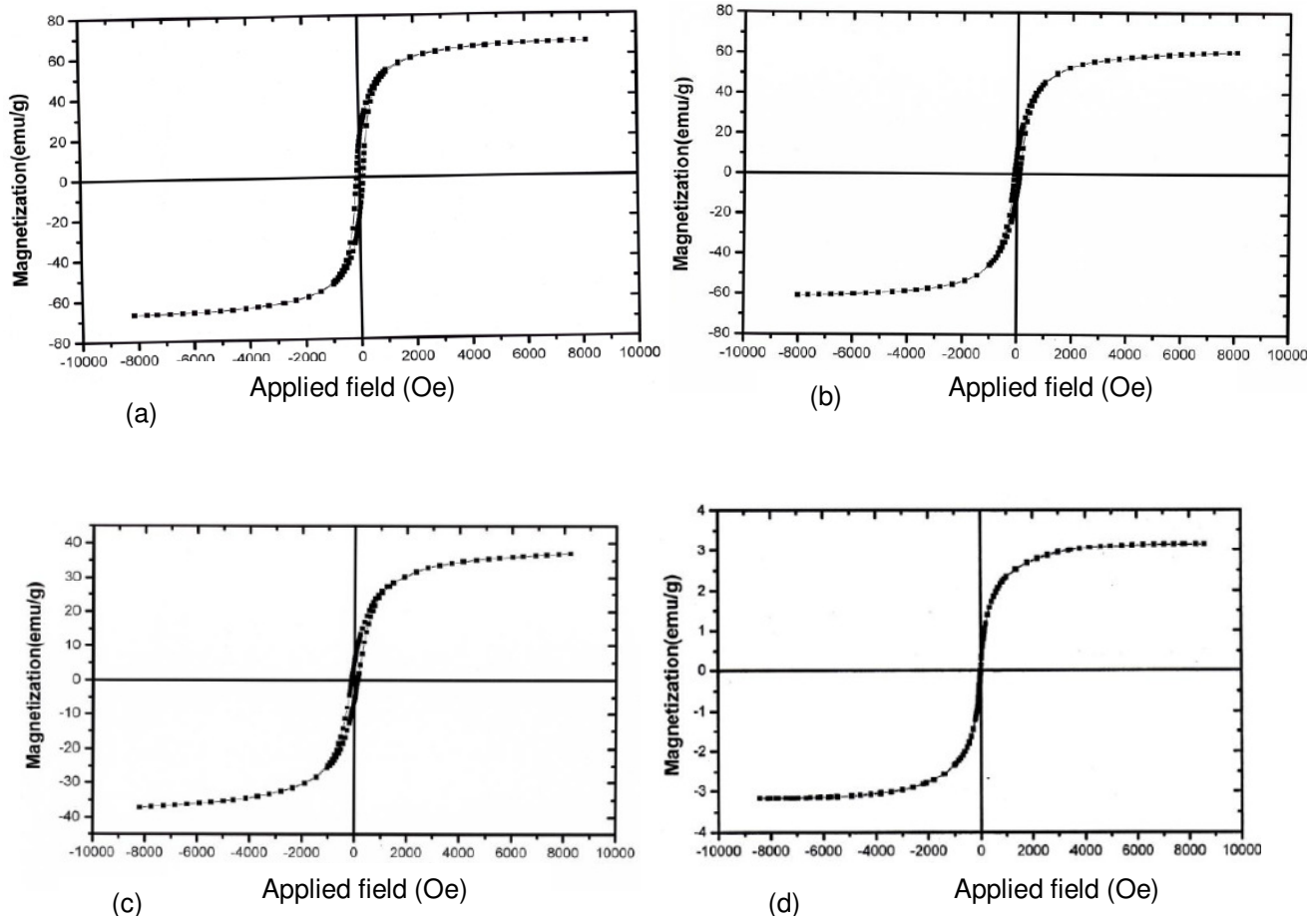

Figure 2. Magnetic hysteresis loop of a) Fe_3O_4 nanoparticle, b) $MnFe_2O_4$ nanoparticle, c) $MnFe_2O_4/Fe_3O_4$ and d) $MnFe_2O_4/Fe_3O_4$-PANi nanocomposites.

changes smoothly with the applied field. This indicates that the $MnFe_2O_4$ core and Fe_3O_4 first shell contact intimately. They are also clearly seen that the value of *Ms* decreases from 66.7 emu/g for Fe_3O_4 to 37emu/g and 60 emu/g for $MnFe_2O_4$ to 37 emu/g for the core-shell structure nanocomposites. And the *Hc* of $MnFe_2O_4/Fe_3O_4$ nanocomposites (155 Oe) is near to Fe_3O_4 (110 Oe) and higher than Fe_3O_4 (110 Oe) and $MnFe_2O_4$ (140 Oe) respectively. The changes in saturation magnetization and the coercivity can be attributed to the existence of Fe_3O_4 on the surface of $MnFe_2O_4$ nanoparticles which can result in the interparticle interaction at the interface of two phases. As saturation magnetization, the interphase interaction leads to the non-collinearity of the magnetic moments at the interface of two phases, and then results in there saturation magnetization (Chen et al., 2007). For coercivity, when the particles contact closely the interphase exchange coupling occurs, with which the rotation of the domains on one particle as the field is reversed, induces domains in contiguous particles to rotate, and thereby decreasing the coercivity (Zhang and Li, 2009; Zeng et al., 2004).

Figure 2d shows clear M_s about 3.15 emu/g, M_r about 0.35 emu/g and *Hc* Oe about 0 for $MnFe_2O_4/Fe_3O_4$/PANi nanocomposite (15 wt%) which is lower than pure ferrite and manganese ferrite nanoparticles. The magnetization curve of the sample shows weak ferromagnetic behavior, with slender hysteresis. Magnetic properties of nanocomposites containing magnetite or ferrite particles have been believed to be highly dependent on the sample shape, crystallinity, and the value of magnetic particles, so that they can be adjusted to obtain optimum property.

Morphology investigation

Figure 3a-c shows the SEM images for a) $MnFe_2O_4$ and b) Fe_3O_4 nanoparticles and $MnFe_2O_4/Fe_3O_4$/PANi nanocomposite. As shown in Figure 3a, the spongy-shaped $MnFe_2O_4$ was seen with a small quantity of amorphous phase. The range of average diameter of spongy-shape is 40 to 50 nm. Figure 3b shows the SEM image for Fe_3O_4 nanoparticles. The range of average

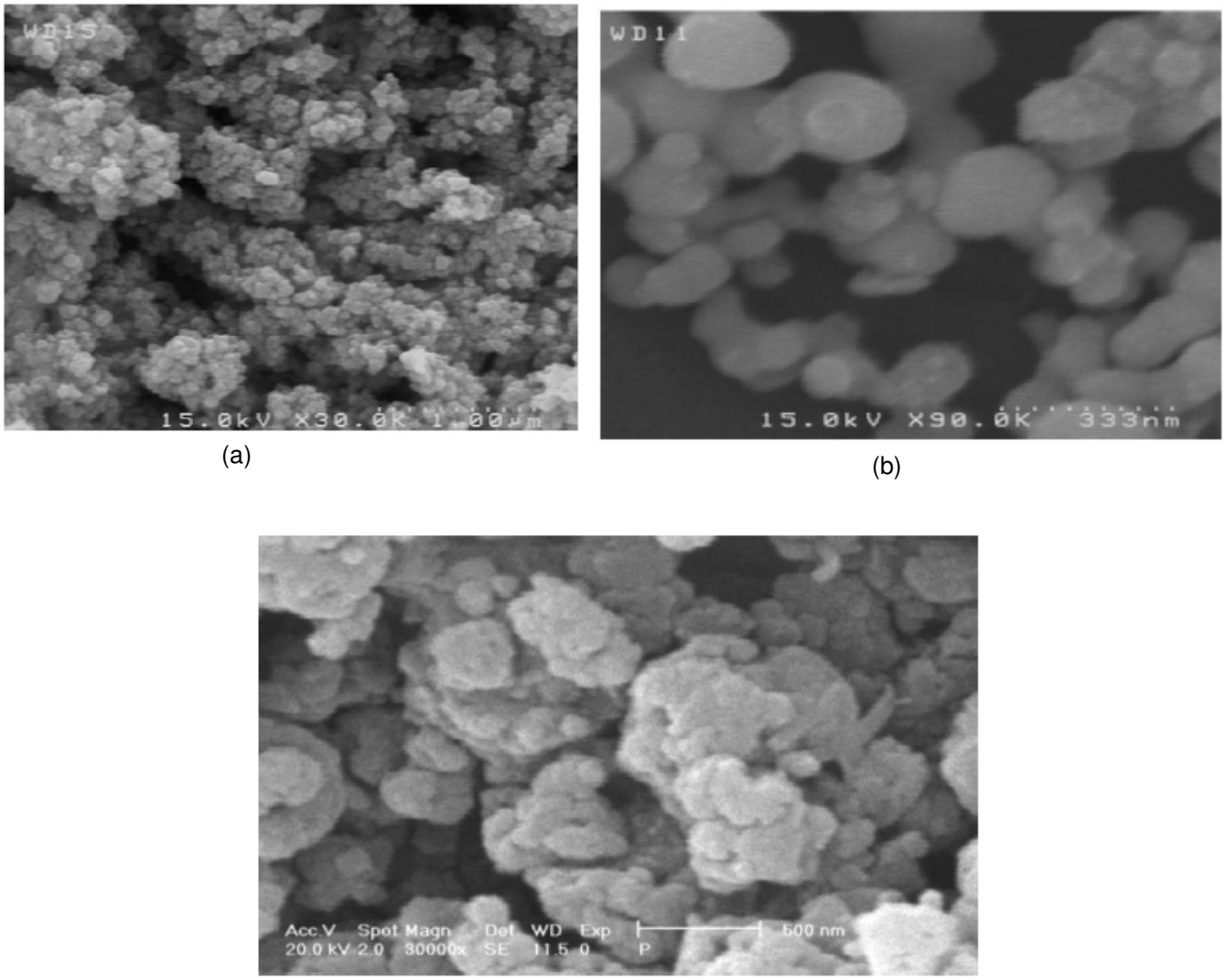

Figure 3. SEM microphotographs of a) Fe_3O_4 nanoparticle, b) $MnFe_2O_4$ nanoparticle and c) $MnFe_2O_4/Fe_3O_4$/PANi nanocomposite.

diameter is 30 to 40 nm. In Figure 3c, it is found that the $MnFe_2O_4/Fe_3O_4$/PANi nanocomposite (15 wt%) still retains the morphology of PANi shape. It is much unknown how to form spongy-shaped composite in the polymerization process. The SEM image clearly shows that the $MnFe_2O_4/Fe_3O_4$ was distributed rather homogeneously, and ultrasonication is effective for dispersing nanoferrite in the polymer matrix.

FTIR spectra analysis

Figure 4a-d shows the FTIR spectra of $MnFe_2O_4$, Fe_3O_4 $MnFe_2O_4/Fe_3O_4$ and $MnFe_2O_4/Fe_3O_4$/PANi nanocomposite, respectively. In ferrites, the metal ions are usually situated in two different sublattices, designated as tetrahedral and octahedral sites according to the geometrical configuration of the oxygen nearest neighbors (Hosseini et al., 2011). It was observed from Figure 4(a,b) that the peak at 578 cm^{-1} is intrinsic vibrations of Fe-O in $MnFe_2O_4$ and peaks at 586 and 411 cm^{-1} are intrinsic vibrations of Fe-O in Fe_3O_4. The peaks at 651 and 562 cm^{-1} are intrinsic vibrations of Fe-O in Fe_3O_4 and $MnFe_2O_4$ have been shown in Figure 4c. The characteristic peaks of styrene occur at 1559, 1338-1067 and 851 cm^{-1}. The peak at 1559 is attributed to the styrene ring. The peak at 1338 cm^{-1} is attributed to the characteristic C=C stretching ring. The peak at 851 cm^{-1} is related to the C–H outer bending vibrations. As shown in Figure 4d, the characteristic peaks of $MnFe_2O_4/Fe_3O_4$/PANi nanocomposite occur at 1555, 1483, 1302, 1241, 1122, 1028, 1002, 876, 800, 675 and 580 cm^{-1}. The peaks at 1555 and 1483 $cm^{-1}$are attributed to the characteristic C=C and C-N stretching of the

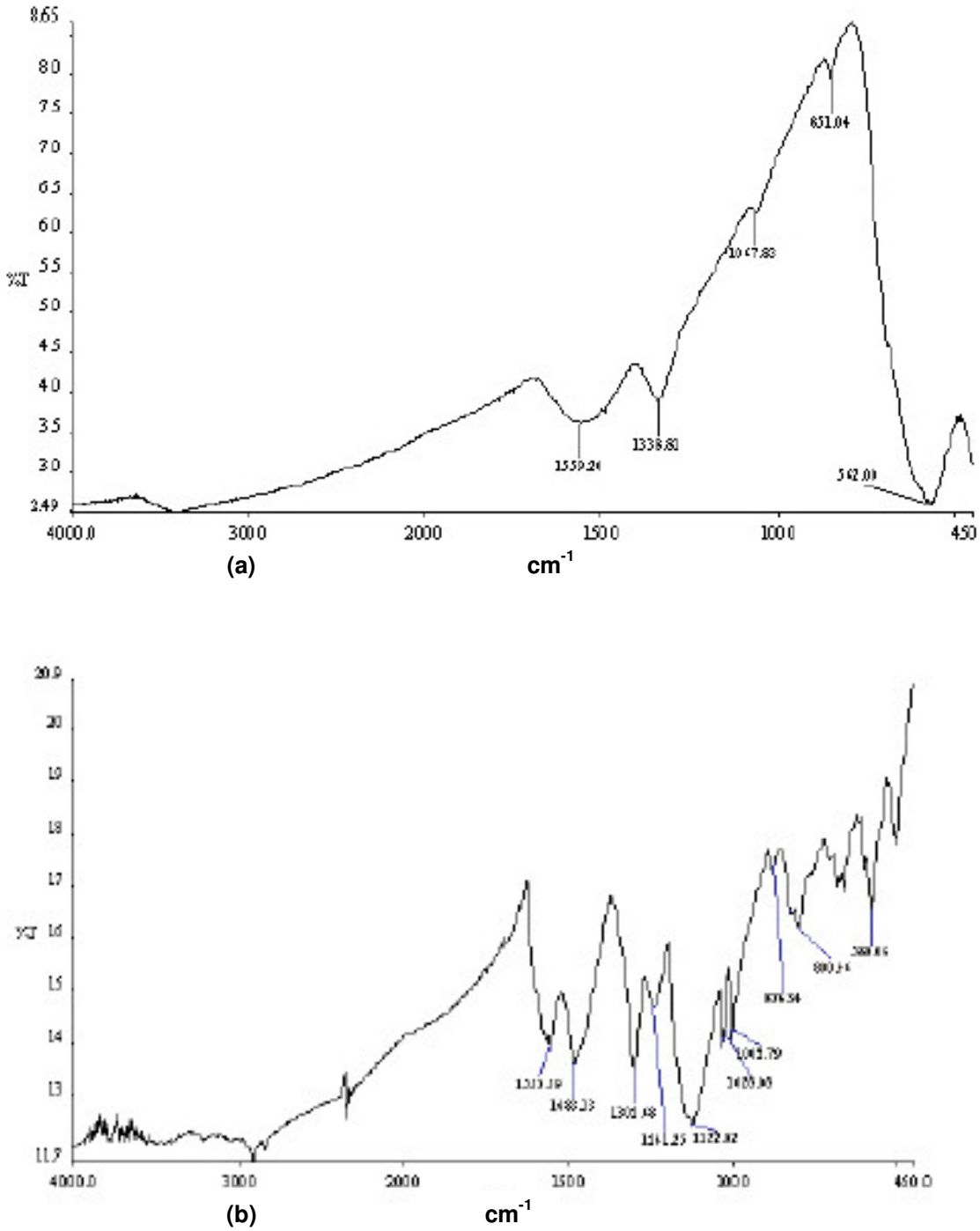

Figure 4. FTIR spectra: a) Fe_3O_4 nanoparticle, b) $MnFe_2O_4$ nanoparticle c) $MnFe_2O_4/Fe_3O_4$ nanoparticle and d) $MnFe_2O_4/Fe_3O_4$/PANi nanocomposite.

quinoid and benzenoid rings of polyaniline; the peaks at 1302 and 1241 cm^{-1} correspond to N–H bending and asymmetric C–N stretching modes of the benzenoid ring. The peak around 1122 cm^{-1} is associated with vibrational modes of N=Q=N (Q refers to the quinonic type rings), indicating that PANi is formed in our sample. The peak at 1028 cm^{-1} attributed to the symmetric and anti-symmetric stretching vibration of SO_3 group of dopant (DBSA). The peaks at1002, 876 and 800 cm^{-1} are attributed to the p-disubstituted aromatic ring C–H out-of-plane bending. However, the characteristic peaks of Fe_3O_4 and $MnFe_2O_4$ can be observed at higher wavenumbers (675 and 580 cm^{-1}) indicating that there is an interaction between $MnFe_2O_4/Fe_3O_4$ nanoparticles and PANi chain.

DC conductivity

DC conductivity of samples at room temperature is shown in Table 1. When the PANi is doped by DBSA, the conductivity was improved to 26 S/cm, which means that doping H^+ increase conductivity of PANi. When 15% mass content of $MnFe_2O_4/Fe_3O_4$ nanoparticles was incorporated, the conductivity of $MnFe_2O_4/Fe_3O_4$/PANi nanocomposite was sharply reduced from 26 to 0.9 S/cm. The decrease in conductivity of $MnFe_2O_4/Fe_3O_4$/PANi composites may be attributed to the insulting behavior of the ferrite and partial blockage of the conductive path by $MnFe_2O_4/Fe_3O_4$ in the core of the nanoparticles (Li et al., 2008b).

Reflection loss analysis

According to transmission line theory, the reflection loss (RL) of electromagnetic radiation, under normal wave incidence at the surface of a single-layer material backed by a perfect conductor can be given by:

$$RL = 20 \log \left| \frac{Z_{in} - Z_0}{Z_{in} + Z_0} \right| \quad (1)$$

where Z_0 is the characteristic impedance of free space,

$$Z_0 = \sqrt{\frac{\mu_0}{\varepsilon_0}} \quad (2)$$

Z_{in} is the input impedance at free space and materials interface:

$$Z_{in} = \sqrt{\frac{\mu_r}{\varepsilon_r}} \tanh \left[j \frac{2\pi f t}{c} \sqrt{\mu_r \varepsilon_r} \right] \quad (3)$$

where μ_r and ε_r are the complex permeability and permittivity of the composite medium respectively, which can be calculated from the complex scatter parameters, c is the light velocity, f is the frequency of the incidence electromagnetic wave and t is the thickness of composites. The impedance matching condition is given by $Z_{in} = Z_0$ to represent the perfect absorbing properties (Chen et al., 2007). There are two different concepts to satisfy the zero reflection condition. The first concept is the ‘‘matched characteristic impedance’’. The intrinsic impedance characteristic of material is made equal to the impedance characteristic of the free space. The second is the ‘‘matched-wave-impedance’’ concept. The wave impedance at the surface of the metallic substrate layer is made equal to the intrinsic impedance of the free space. In this work, the second concept was applied. The condition of maximal absorption is satisfied at a particular point where thickness and frequency match each other. Ferrites are the only materials that present two matching frequencies and thicknesses. The first matching at low-frequency is associated with the mechanisms of magnetic resonance and shows a dependence on the chemical composition. The second matching at high-frequency is associated with the thickness of absorbent material. To satisfy the zero-reflection condition where maximum absorption would occur, Z_{in} should be 1 to prevent reflection. This can be ideally achieved when the material presents $|\mu_r| = |\varepsilon_r|$. In this case, the performance of electromagnetic wave-absorbing material increases linearly with the increase in thickness. In practical terms, however, this is rarely achieved because the values of complex permeability and complex permittivity are very different in the frequency range of interest. When $|\mu_r| \neq |\varepsilon_r|$, we should consider two other cases. For materials with intrinsic impedances greater than unity, $|\mu_r| > |\varepsilon_r|$, the minimum reflection loss occurs at around a half-wavelength thickness of the material, and for materials with intrinsic impedances lower than unity, $|\mu_r| < |\varepsilon_r|$, the minimum reflection loss occurs at around a quarterwavelength thickness of the material. Within the microwave region, ferrites usually present electromagnetic characteristics of $|\mu_r| \ll |\varepsilon_r|$, giving rise to the term ‘‘quarter-wavelength absorbent’’. Minimum loss occurs when the thickness is about an odd multiple of one quarter of the wavelength of the incident frequency. It measured inside the absorbing material, and the material has the proper loss factor for this particular thickness .The thickness, d, can be written as Equation (4), where c is the speed of light and f is the frequency of interest (Bueno et al., 2008).

$$d = \frac{c}{4f\sqrt{|\mu_r||\varepsilon_r|}} \quad (4)$$

Investigation of microwave absorbing properties

Nanocomposite dispersed in acrylic resins then the mixture was pasted on metal plate with the area of 100 ×100 mm as the test plate. The microwave absorbing properties of the nanocomposite with the coating thickness of 1 mm were investigated by using a HP 8720B vector network analyzer and standard horn antennas in anechoic chamber in the frequency range of 8–12 GHz. Figure 5 shows the microwave absorption behavior of the $MnFe_2O_4/Fe_3O_4$/PANi nanocomposite. For PANi with the coating thickness of 1 mm, the minimum reflection loss is -8 dB at the frequency of 8-12 GHz. For $MnFe_2O_4/Fe_3O_4$/PANi nanocomposites with the coating thickness of 1 mm, the reflection loss values were obtained less than -10 dB in the frequency of 8–12 GHz and its value of minimum reflection loss are -18 and -17 dB at the frequency of 8.6 and 9.2 GHz, respectively. Compared with the core-shell $MnFe_2O_4$/PANi (-15.3 dB at 10.4 GHz) (Hosseini et al., 2011) and the new multi core-

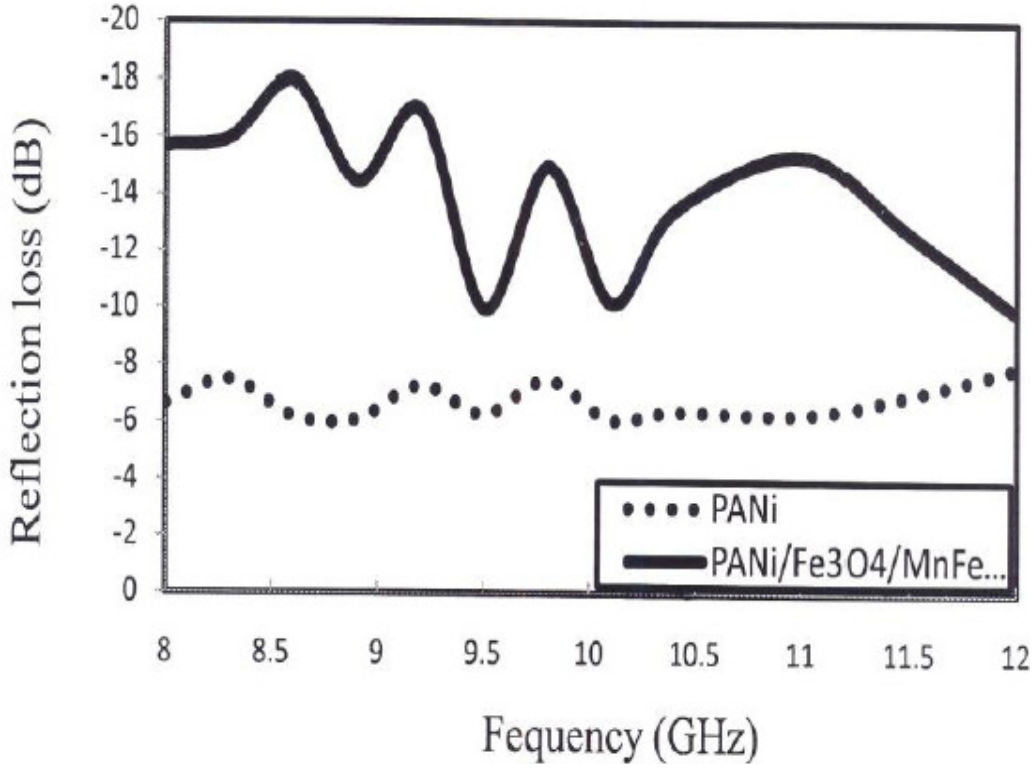

Figure 5. Frequency dependence of RL for the $MnFe_2O_4$/PANi nanocomposite.

shell $MnFe_2O_4/Fe_3O_4$/PANi nanocomposite (-18 dB at 8.6 GHz and -17 dB at 0.2 GHz), the microwave absorption properties of multi core-shell structure nanocomposite have been improved effectively. The reason for this improvement may be due to the interphase interaction between the cubic $MnFe_2O_4$ and cubic ferrite Fe_3O_4. These two kinds of ferrite combine intimately with the two step co-precipitation synthetic method, so they can couple to each other by an exchange through interface of ferrite particles. The interphase interaction which can cause the interphase exchange coupling and the non-collinearity of the magnetic moments at the interface of two phases exists between cubic ferrite materials. The interphase interaction can affect the microwave absorption properties of the two-phase composites had been shown in previous study (Zhang and Li, 2009). As mentioned above, the results of this work are consistent with these previous reports.

Conclusion

The obtained magnetic nanoparticles are of a diameter of 24.27, 7.38 and 31.65 nm for $MnFe_2O_4$, Fe_3O_4 and $MnFe_2O_4/Fe_3O_4$, respectively. $MnFe_2O_4/Fe_3O_4$/PANi ferrite nanocomposite with the magnetic behavior is successfully synthesized by *in situ* polymerization of aniline in the presence of $MnFe_2O_4/Fe_3O_4$ nanoparticles. The results of spectro-analysis indicate that there is an interaction between PANi chain and ferrite particles. Furthermore; for 1 mm thickness of nanocomposite used, a minimum reflection loss of -18 and -17 dB were observed at 8.6 and 9.2 GHz, respectively. Journal of Nanomaterials, Vol. 2012, 1687-4110 (2012).

REFERENCES

Bueno AR, Gregori M, No´brega MCS (2008). Microwave-absorbing properties of $Ni_{0.50-x}Zn_{0.50-x}Me_{2x}Fe_2O_4$ (Me=Cu, Mn, Mg) ferrite–wax composite in X-band frequencies, J. Magn. Magn. Mat. 320:864-870.

Chen N, Mu GH, Pan XF, Gan KK, Gu MY (2007). Microwave absorption properties of $SrFe_{12}O_{19}/ZnFe_2O_4$ composite powders, Mater. Sci. Eng. B 139:256-260.

Farghali AA, Moussa M, Khedr MH (2010). Synthesis and characterization of novel conductive and magnetic nanocomposites, J. Alloys Comp. 499:98–103.

Hosseini SH, Mohseni SH, Asadnia A, Kerdari K. (2011). Synthesis; characterization and microwave absorbing properties of polyaniline/$MnFe_2O_4$ nanocomposite, J. Alloys Comps. 509:4682-4687.

Li X, Han X, Tan Y, Xu P (2008a). Preparation and microwave absorption properties of Ni–Balloy-coated Fe_3O_4 particles, J. Alloys Comp. 464:352–356.

Li Y, Zhang H, Liu Y, Wen Q, Li J (2008b). Rod-shaped polyaniline–barium ferrite nanocomposite: preparation, characterization and properties, Nanotechnology, 19:105605-105610.

Phang SW, Tadokoro M, Watanabe J, Kuramoto N (2008). Microwave absorption behaviors of polyaniline nanocomposites containing TiO_2 nanoparticles, Cur. Appl. Phys. 8:391–394.

Xiao HM, Liu XM, Fu SY (2006). Synthesis, magnetic and microwave

absorbing properties of core-shell structured $MnFe_2O_4/TiO_2$ nanocomposites, Comp. Sci. Tech. 66:2003-2008.
Yang C, Li H, Xiong D, Cao Z (2009). Hollow polyaniline/Fe_3O_4 microsphere composites: Preparation, characterization, and applications in microwave absorption, Reactive Functional Polym. 69:137–144.
Zeng H, Sun S, Li J, Wang ZL, Liu JP (2004). Tailoring magnetic properties of core/shell nanoparticles, Appl. Phys. Lett. 85:792-794.
Zhang L, Li Z (2009). Synthesis and characterization of $SrFe_{12}O_{19}/CoFe_2O_4$ nanocomposites with core-shell structure, J. Alloys Comp. 469:422–426.